

Numerical Study on the Effect of Current Profiles on Vortex-Induced Vibrations in a Top-Tension Riser

Bowen Fu, Lu Zou and Decheng Wan*

State Key Laboratory of Ocean Engineering, School of Naval Architecture, Ocean and Civil Engineering, Shanghai Jiao Tong University, Collaborative Innovation Center for Advanced Ship and Deep-Sea Exploration, Shanghai 200240, China

Abstract: In this paper, numerical simulations of vortex-induced vibrations in a vertical top-tension riser with a length-to-diameter ratio of 500 using our in-house code viv-FOAM-SJTU are presented. The time-dependent hydrodynamic forces on two-dimensional strips are obtained by solving the Navier-Stokes equations, which are, in turn, integrated into a finite-element structural model to obtain the riser deflections. The riser is discretized into 80 elements with its two ends set as pinned and 20 strips are located equidistant along the risers. Flow and structure are coupled by hydrodynamic forces and structural displacements. In order to study the effects of the shear rate, of the current profiles on the vortex-induced vibrations in the riser, vibrations, with varying shear rates, in both the in-line and cross-flow directions, are simulated. In addition to the time domain analysis, spectral analysis was conducted in both the temporal and spatial domains. Multi-mode vibration characteristics were observed in the riser. The relationship between dominant vibration mode number and the shear rate of current profiles is discussed. In general, the overall vibrations in the riser pipe include contributions from several modes and each mode persists over a range of shear rates. Moreover, the results suggest that with a larger shear rate the position of the maximum in-line time-averaged displacement will move closer to the end where the largest velocity is located.

Keywords: risers, vortex-induced vibration, multi-modal vibration, strip theory, computational fluid dynamics, fluid-structure interaction

Article ID: 1671-9433(2017)04-0473-07

1 Introduction

Vortex-Induced Vibration (VIV) is a problem of concern in ocean engineering. With oil exploitation moving to deeper seas, the length-to-diameter ratio of risers has reached the magnitude of 10^3 (Willden and Graham, 2001). One feature of long risers is their high mode vibration. A subtle difference with rigid cylinders is that synchronization competes with

multi-mode response due to excitation frequency mismatching along the span (Lucor *et al.*, 2001). Experimental studies on long risers subject to various current profiles have been undertaken (Chaplin *et al.*, 2005a; Chaplin *et al.*, 2005b; Gu *et al.*, 2013; Huera-Huarte, 2006; Huera-Huarte *et al.*, 2006; Huera-Huarte and Bearman, 2009a; Huera-Huarte and Bearman, 2009b; Huera-Huarte *et al.*, 2014; Huera-Huarte *et al.*, 2016; Gu *et al.*, 2013; Song *et al.*, 2016). Multi-mode vibrations and mode transitions were observed in these model tests. In numerical work, empirical modeling and Computational Fluid Dynamics (CFD) are two common ways to predict vortex-induced vibrations in long risers. This includes work by: Willden and Graham (2001, 2004, 2006), Srinil (2010), Gu and Duan (2016), Pavlovskaja *et al.* (2016), Rahman *et al.* (2016), Wang and Xiao (2016), Monreal-Jiménez *et al.* (2016), and Klaycham *et al.* (2016).

An efficient scheme to simulate VIV is based on the strip theory (Willden and Graham, 2004; Willden *et al.*, 2001), and this was adopted in the current work. The solver viv-FOAM-SJTU based on the strip theory was developed on the open source software OpenFOAM. To study the effects of current profiles, in this present work we numerically investigated VIV in a vertical top-tension riser subject to shear flows with various shear rates using our in-house code viv-FOAM-SJTU.

2 Numerical methods

The flow field was computed by solving transient incompressible Reynolds-averaged Navier-Stokes equations

$$\frac{\partial \bar{u}_i}{\partial x_i} = 0 \quad (1)$$

$$\rho \frac{\partial \bar{u}_i}{\partial t} + \rho \frac{\partial}{\partial x_j} (\overline{u_i u_j}) = -\frac{\partial \bar{p}}{\partial x_i} + \frac{\partial}{\partial x_j} (2\mu \bar{S}_{ij} - \rho \overline{u_i u_j}) \quad (2)$$

where the mean strain tensor $\bar{S}_{ij} = \frac{1}{2} \left(\frac{\partial \bar{u}_i}{\partial x_j} + \frac{\partial \bar{u}_j}{\partial x_i} \right)$ and

$-\overline{u_i u_j}$ is the Reynolds stress tensor, consisting of six independent variables. Transient values can be decomposed into mean values and fluctuations, thus introducing three unknowns. To model the Reynolds stress, the Boussinesq hypothesis was adopted to relate Reynolds stress to mean

Received date: 13-Dec-2016

Accepted date: 04-Jun-2017

Foundation item: Supported by the National Natural Science Foundation of China (51379125, 51490675, 11432009, 51579145), Chang Jiang Scholars Program (T2014099), Shanghai Excellent Academic Leaders Program (17XD1402300), Program for Professor of Special Appointment (Eastern Scholar) at Shanghai Institutions of Higher Learning (2013022), Innovative Special Project of Numerical Tank of Ministry of Industry and Information Technology of China (2016-23/09) and Lloyd's Register Foundation for Doctoral Student

*Corresponding author Email: dcwan@sjtu.edu.cn

© Harbin Engineering University and Springer-Verlag GmbH Germany 2017

velocity gradients. An SST k-omega model was used for turbulence closure (Menter, 1994; Menter *et al.*, 2003). No wall functions are used in the present work. Instead a refined mesh close to the cylinder is used to predict turbulence kinetic energy close to the cylinder (Chien, 1982; Wilcox, 1993). A CFD model based on strip theory, with two-dimensional strips located equidistantly along the span, was adopted to simulate the flow field. The PIMPLE (merged PISO-SIMPLE) algorithm in OpenFOAM was used, which applies to transient incompressible flow.

The riser was modeled as a small displacement Bernoulli–Euler bending beam, with two ends set as pinned. The tension varies along the span due to gravity, but not temporally. In the finite element analysis, we have

$$M\ddot{x} + C\dot{x} + Kx = F_{Hx} \tag{3}$$

$$M\ddot{y} + C\dot{y} + Ky = F_{Hy} \tag{4}$$

where x and y are nodal displacement vectors, the point denotes the derivative with respect to time, M , C , K are the mass, damping, and stiffness matrices, and F_{Hx} and F_{Hy} are fluid forces. The equations were solved using the Newmark-beta method (Clough and Penzien, 2003).

At the beginning of each time step hydrodynamic forces were mapped to structural model nodes to compute the riser displacement. Next, the mesh was deformed accordingly and a new flow field obtained. In this way, the time step was advanced. The procedure is shown in Fig. 1, the solver viv-FOAM-SJTU (Duan *et al.*, 2016) was formed based on this. The 3D structural dynamics analysis and 2D RANS CFD analysis are coupled by hydrodynamic forces and structural deflections. The motion solver “displacementLaplacian” in OpenFOAM is applied to handle the dynamic mesh (Jasak, 2009).

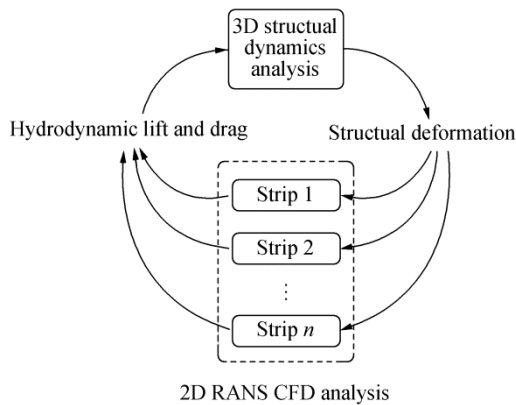


Fig. 1 Fluid-structure interaction procedure in viv-FOAM-SJTU code

3 Numerical simulation setup

Huera-Huarte (2006) conducted a series of model tests of a riser exposed to a stepped current, with the lower 45% of the riser exposed to a uniform current and the upper part in still water. A numerical simulation of the same model with identical parameters using viv-FOAM-SJTU has been

performed by Duan *et al.* (2016); the results appear to agree well with the experiment.

A similar model riser was used in the present work. The main parameters are listed in Table 1. All cases considered here share the same parameters and include the span-averaged current speed \bar{V} , with a shear rate $S = (V_{max} - V_{min}) / \bar{V}$ varying from 0 to 0.75. The current speed reaches its maximum value at $z/L = 0$ and minimum at $z/L = 1$. The shear current profiles are linear along the span.

Table 1 Main parameters of simulations

Items	Values
Mass ratio m^*	2.4
Mean current speed $\bar{V}/(\text{m}\cdot\text{s}^{-1})$	0.4
Diameter D/m	0.028
Length L/m	14
Bending stiffness $EI/(\text{N}\cdot\text{m}^2)$	29.88
Top tension T_t/N	1 610

The twenty strips along the span are shown in Fig. 2. The initial mesh of the flow field on each strip is shown in Fig. 3. The Inlet is 15 diameters before the riser axis and the outlet 30 diameters behind the riser axis; both sides 15 diameters away from the axis. Imposed on the surface of the riser is a no-slip boundary. At the inlet the normal velocity is the given current speed and the pressure gradient is zero, while at the outlet the normal velocity gradient and the relative pressure are both zero. The normal velocities and pressure gradients on both sides are zero. Vortex shedding alternately behind the riser can be seen clearly in Fig. 4. Drag forces induce in-line vibrations while lift forces lead to cross-flow vibrations. Fig. 5 shows the structural elements. The riser is discretized into 80 elements, and each element has an imposed uniformly distributed load. Plotted in Fig. 6 are the first seven mode shapes of the riser, with the corresponding natural frequencies listed in Table 2.

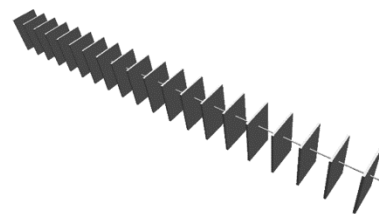


Fig. 2 Twenty strips located equidistant along the span of the riser

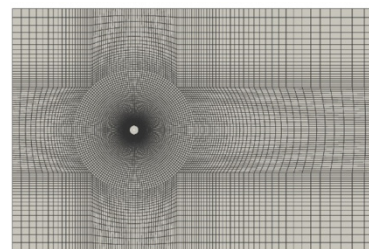


Fig. 3 Initial mesh on each strip

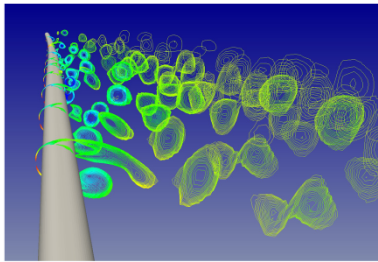


Fig. 4 Vortex shedding alternately behind the riser

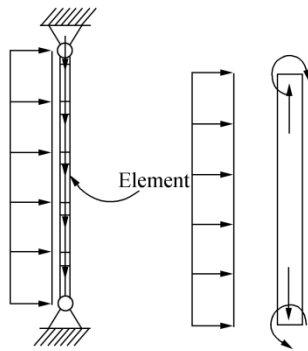


Fig. 5 Structural model of the vertical riser

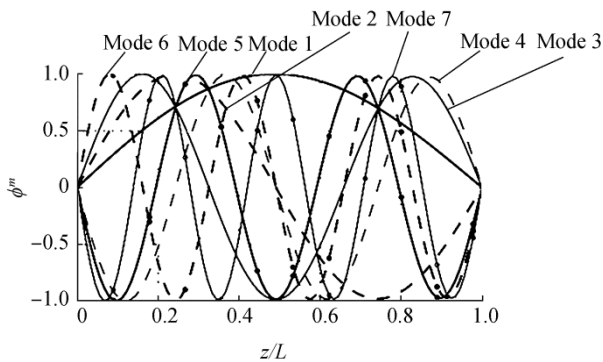


Fig. 6 First seven mode shapes

Table 2 Main parameters of simulations

f_n^1	f_n^2	f_n^3	f_n^4	f_n^5	f_n^6	f_n^7
1.14	2.29	3.44	4.60	5.77	6.97	8.18

4 Simulation results

4.1 A typical case

First, we focus on a typical case with a shear rate $S = 0.5$. In the following figures, most values are non-dimensionalized with respect to the riser diameter D except the elevation z , which gets dimensionless with respect to the riser length L .

The in-line time-averaged displacement along the span z/L is presented in Fig. 7 (a), reflecting clearly the effect of current drag force. The in-line time-averaged curvature in Fig. 7(b) reflects the mean position of the in-line vibration from another perspective, showing the effect of shear rate. The standard deviations of in-line displacement and curvature with respect to time are presented in Figs. 7 (c) and (d). Fig. 8

shows the standard deviations of cross-flow displacement and curvature with respect to time. The dominant vibration modes can be seen clearly from the standard deviations of the curvatures. The dominant mode numbers are 6 and 3 in in-line and cross-flow directions, respectively. The small but nonzero standard deviations of both the in-line and cross-flow displacements never reach zero for any nodes except the two end ones, indicating that the seeming standing nodes move somewhat in time and no pure standing wave exists.

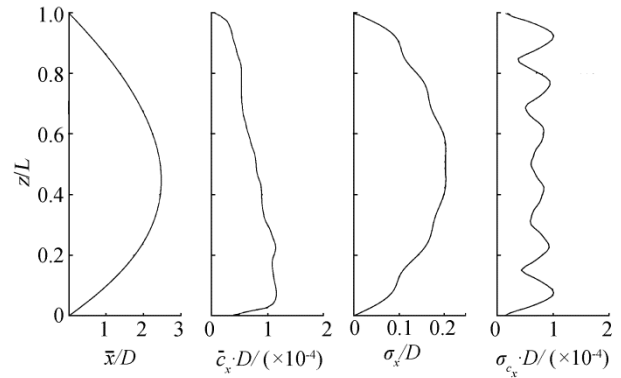


Fig. 7 Time-averaged values and standard deviations of in-line displacement and curvature

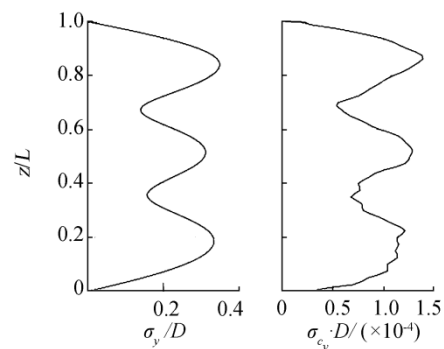
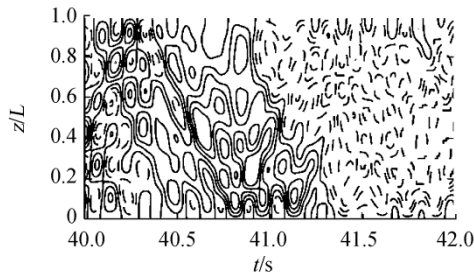


Fig. 8 Standard deviations of cross-flow displacement (σ_y/D) and curvature ($\sigma_{\epsilon_y} \cdot D$)

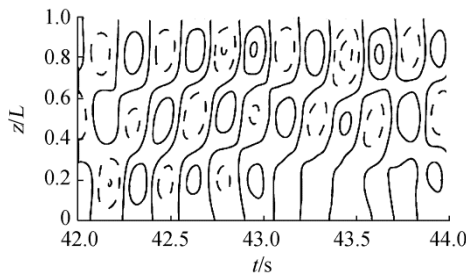
The spatio-temporal contours in Fig. 9 describe the time-varying and space-varying features of VIV. The characteristics of a traveling wave can be observed. The low-frequency first-order modal vibration in the in-line direction influences the in-line displacement significantly.

Contours of the displacement power spectral densities are presented in Fig. 10. Representing the cross-flow motion in spectral space, we see that only one dominant mode is excited, i.e., the 3rd mode, though with a slightly wide envelope of frequencies. The dominant vibration frequency is near 3 Hz. From Table 2, it is known that the 3rd undamped natural frequency is 3.44 Hz, i.e., the actual vibration frequency is about 0.86 of the corresponding undamped natural frequency. This discrepancy may be due to damping. For the in-line vibration, a lower peak exists beside the dominant frequency and shows a multi-mode frequency response, with a dominant

mode number of 6 and a secondary mode number of 7. The nodes expected to be standing points for the 6th mode, actually vibrate at the 7th mode.

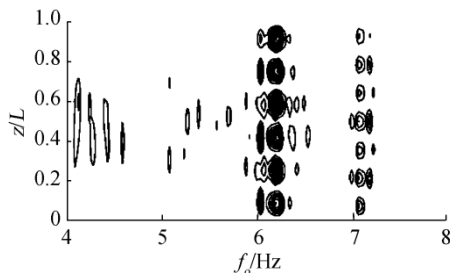


(a) In-line vibration with the 6th dominant mode

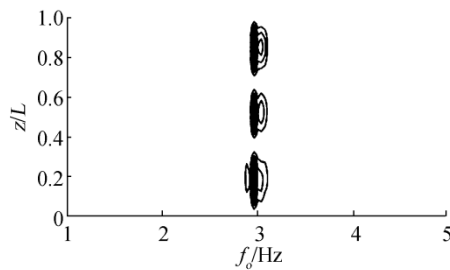


(b) Cross-flow vibration with the 3rd dominant mode

Fig. 9 Spatio-temporal contours of displacements. Solid and dashed lines denote the two sides of the time-averaged position



(a) In-line vibration



(b) Cross-flow vibration

Fig. 10 Power spectral density contours

Figs. 11 and 12 show the modal compositions of vibrations along with their corresponding spectrum. At any instance, the mode with the highest modal weight is considered the dominant mode. The least-squares method (Trim *et al.*, 2005; Lie and Kaasen, 2006) was used to conduct modal decomposition. The deflected shape of the riser was

represented in spectral terms, i.e., the entire riser's displacement was decomposed into modal contributions through

$$x = \phi u \tag{5}$$

$$y = \phi v \tag{6}$$

where ϕ is the matrix of mode shapes, and u, v are the modal weights of x and y . Trim *et al.* (2005) and Lie and Kaasen (2006) suggested conducting modal decompositions in the least-squares sense using

$$\phi^T x = \phi^T \phi u \tag{7}$$

$$\phi^T y = \phi^T \phi v \tag{8}$$

where only those desirable mode shapes are included in ϕ .

The most distinguishing feature of the in-line vibration is the transition between the 6th and 7th modes. The 7th mode dominates the vibration from 35 to 36 s. The corresponding dominant mode transition from the 7th to the 6th mode at 36 s can be observed evidently in Fig. 11. There is also a short period of the 4th mode-dominated time for cross-flow vibrations near 35 s, while the 3rd mode dominates the vibration at other times.

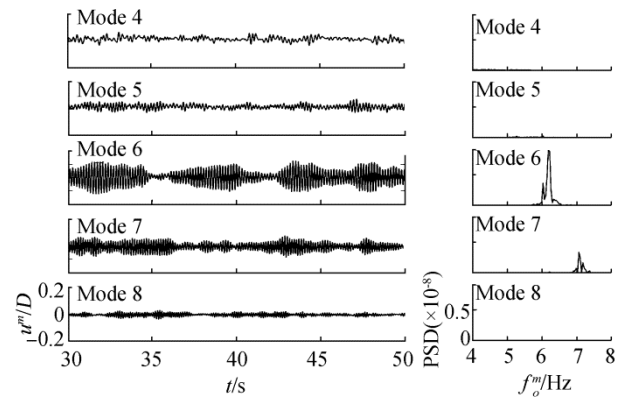


Fig. 11 In-line modal weights u^m/D and corresponding power spectral densities, and the 6th mode is the dominant mode

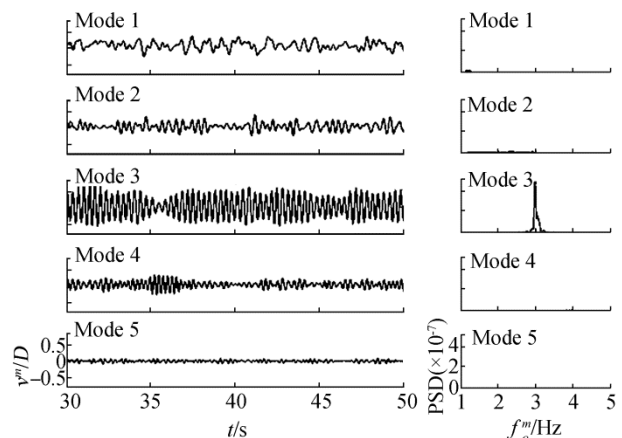


Fig. 12 Cross-flow modal weights v^m/D and corresponding power spectral densities, and the 3rd mode is the dominant mode

4.2 Effects of shear rates

To determine the relationship between the overall response and shear rate, all cases simulated with shear rates varying from 0 to 0.75 were plotted together. Figs. 13 and 14 show the root mean square values of the modal weights of the cross-flow and in-line displacements of selected cases, respectively. For $S = 0.1, 0.3, 0.5$ the vibrations are dominated by the 3rd mode in the cross-flow direction, while for the $S = 0.7$ both the 3rd and the 4th modes contribute considerably. As for the in-line vibration, for $S = 0.7$ the 7th mode dominates the response while the other three cases stick to the 6th mode.

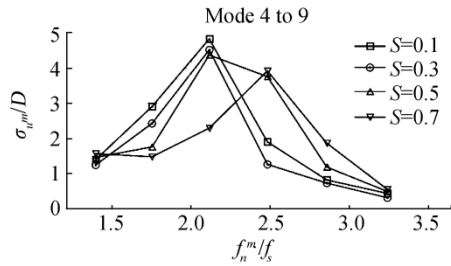


Fig. 13 Standard deviations σ_{u^m} / D of in-line displacement modal weights

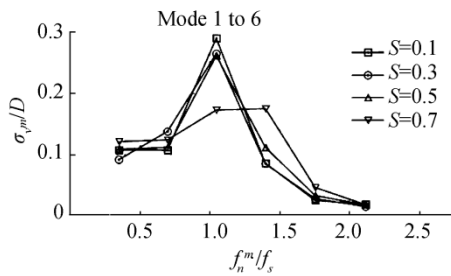


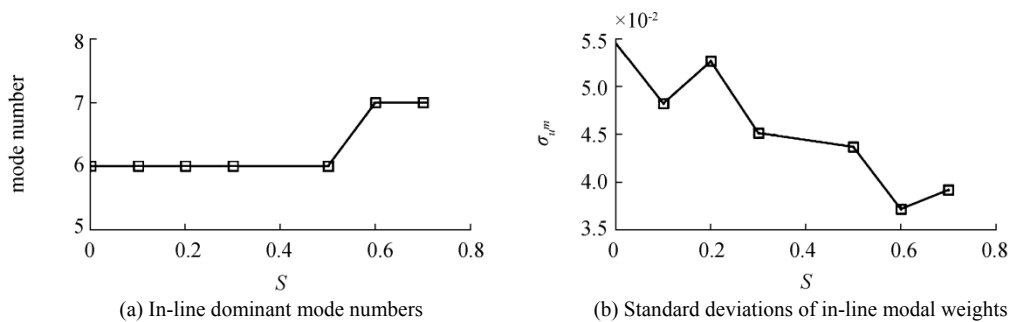
Fig. 14 Standard deviations σ_{v^m} / D of cross-flow displacement modal weights

The Strouhal frequency used in Figs. 13 and 14 is based on the span-averaged current speed from the sheared inflow, i.e., $f_s = St\bar{V} / D = 2.86 \text{ Hz}$, as $St = 0.2$ for $Re = 11\ 200$. When the shear rate is low, the cross-flow dominant mode is confined to the modes with natural frequencies close to the span-averaged Strouhal frequency, and the in-line dominant mode is confined to the modes with natural frequencies close to twice the span-averaged Strouhal frequency. Actually, when shear rate S reaches zero, this span-averaged Strouhal

frequency is exactly the actual Strouhal frequency at any position along the riser. However, when shear rate S is high, such as $S = 0.7$, the coupled flow structure system has a frequency response that deviates toward a larger value from this span-averaged Strouhal frequency. For $S = 0.7$, the riser vibrates mainly at the 4th mode in the cross-flow direction, whose natural frequency is close to $1.5f_s = 4.29 \text{ Hz}$. And the Strouhal frequency based on the maximum current speed is exactly 4.29 Hz . This shows that the maximum current speed has an important effect on the dominant mode.

Fig. 15 shows the dominant mode numbers of the vibrations and the standard deviations of the modal weights σ_{u^m} / D and σ_{v^m} / D plotted against increasing shear rate. The general tendency is that dominant mode numbers increase with larger shear rates. It can be seen that with shear rates S varying from 0 to 0.5 the dominant mode number still keeps constant, indicating that the effect of shear rate on the dominant mode number is limited. The standard deviations of the modal weights of the dominant modes are very low when the dominant mode is shifted, i.e., for a shear rate S of 0.6 in the in-line direction and 0.7 in the cross-flow direction. Fig. 16 shows the dominant vibration frequencies (the root mean square value of the dominant vibration frequencies along the span) with increasing shear rate. It seems that the dominant vibration frequencies in both directions tend to increase with shear rate.

This is reasonable because a larger shear rate denotes that the largest current speed in that case has become larger. It is known that in stepped currents part of the riser is in still water. But that part will still vibrate and the vibration is dominated by the current experienced by the other part, i.e., the vibration travels from the part exposed to currents to the rest. The stepped current can be considered as a special type of shear current. When shear rate increases and the span-averaged current speed remains constant, the maximum current speed increases. A larger maximum current speed means larger energy input, resulting in a higher dominant mode. Actually, how the distribution of the input energy affects vibration deserves more research. For certain current profiles the energy input at a different position may balance that at another position. This may help explain why cross-flow dominant vibration frequency drops noticeably for $S = 0.3$.



(a) In-line dominant mode numbers

(b) Standard deviations of in-line modal weights

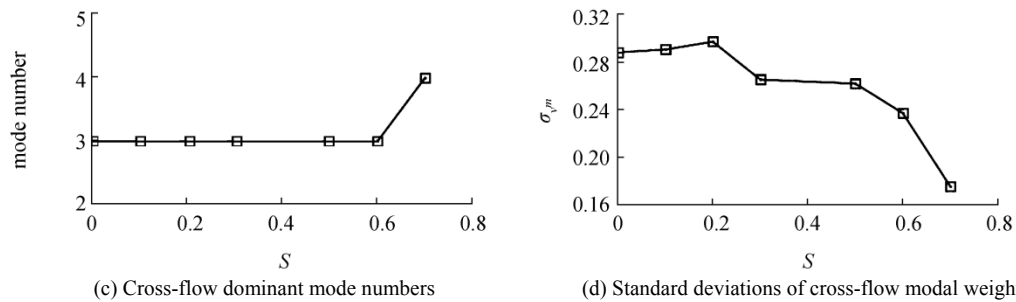


Fig. 15 Dominant mode numbers and standard deviations of the modal weights with increasing shear rates S

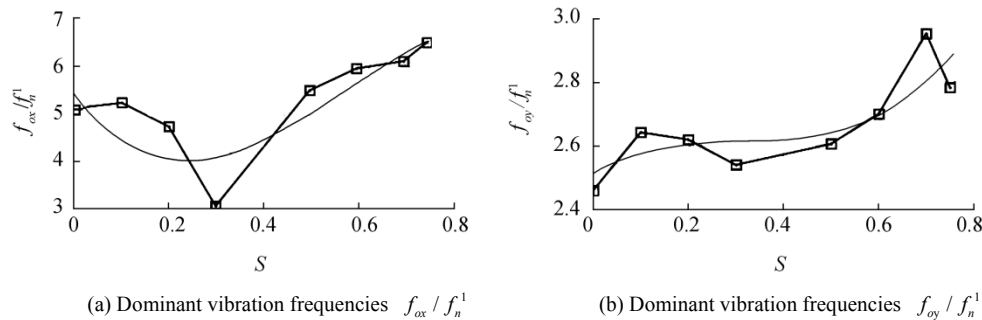


Fig. 16 Dominant vibration frequencies with increasing shear rates S

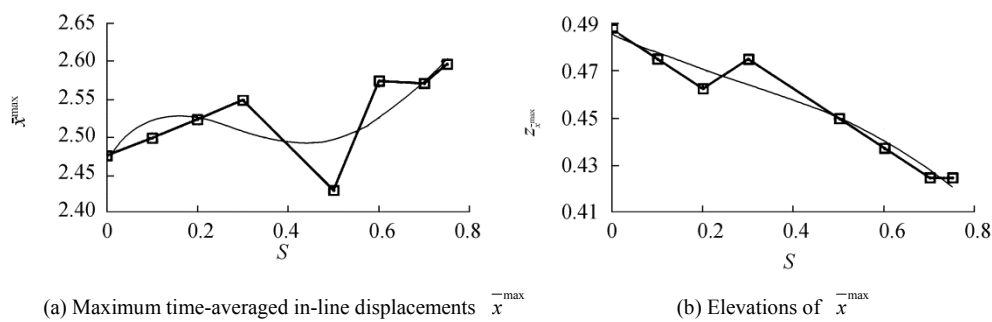


Fig. 17 Maximum time-averaged in-line displacements along the span and corresponding elevations

Fig. 17 shows the maximum time-averaged in-line displacements and the positions where the maximum value is obtained. Though no clear relationship is seen between maximum displacement and shear rate, a slight shift of position toward the side of high inflow with increasing shear rate can be observed. The maximum structural response of the beam is reached on the side of high inflow.

5 Conclusions

A series of numerical studies, using our in-house code viv-FOAM-SJTU based on strip theory, have been performed for the vortex-induced vibrations of a 14 m long top-tensioned model riser with a diameter of 28 mm. Using various shear rates, the simulations were designed to explore the effects of the shear rate of the current profile on the VIV of the riser. It was found that shear rates do not affect the dominant vibration mode much. However, there is a slight positive correlation between dominant vibration mode number and shear rate. In general, the overall vibration of the riser pipe includes contributions from several modes,

and each mode persists over a range of shear rates. The traveling wave characteristic of the vibration was observed. Moreover, the results suggest that with a larger shear rate the position of the largest in-line time-averaged displacement will move closer to the end where the largest current speed is located.

References

- Chaplin JR, Bearman PW, Cheng Y, Fontaine E, Graham JMR, Herford K, Meneghini JR, 2005a. Blind predictions of laboratory measurements of vortex-induced vibrations of a tension riser. *Journal of Fluids and Structures*, **21**(1), 25-40. DOI: 10.1016/j.jfluidstructs.2005.05.016
- Chaplin JR, Bearman PW, Huarte FH, Pattenden RJ, 2005b. Laboratory measurements of vortex-induced vibrations of a vertical tension riser in a stepped current. *Journal of Fluids and Structures*, **21**(1), 3-24. DOI: 10.1016/j.jfluidstructs.2005.04.010
- Chien K, 1982. Predictions of channel and boundary-layer flows with a low-Reynolds-number turbulence model. *AIAA Journal*. **20**(1), 33-38.

- Clough RW, Penzien J, 2003. *Dynamics of structures*. Computers & Structures, Inc., Berkeley, 121.
- Duan M, Wan DC, Xue H, 2016. Prediction of response for vortex-induced vibrations of a flexible riser pipe by using multi-strip method. *Proceedings of the 26th International Ocean and Polar Engineering Conference*, Rhodes, Greece, 1065-1073.
- Gu J, Duan M, 2016. Integral transform solution for fluid force investigation of a flexible circular cylinder subject to vortex-induced vibrations. *Journal of Marine Science and Technology*, **21**(4), 663-678.
DOI: 10.1007/s00773-016-0381-2
- Gu J, Vitola M, Coelho J, Pinto W, Duan M, Levi C, 2013. An experimental investigation by towing tank on VIV of a long flexible cylinder for deepwater riser application. *Journal of marine science and technology*, **18**(3), 358-369.
DOI: 10.1007/s00773-013-0213-6
- Huera-Huarte FJ, 2006. *Multi-mode vortex-induced vibrations of a flexible circular cylinder*. PhD thesis, Imperial College London (University of London), London, 20-60.
- Huera-Huarte FJ, Bangash ZA, Gonzalez LM, 2014. Towing tank experiments on the vortex-induced vibrations of low mass ratio long flexible cylinders. *Journal of Fluids and Structures*, **48**, 81-92.
DOI: 10.1016/j.jfluidstructs.2014.02.006
- Huera-Huarte FJ, Bangash ZA, González LM, 2016. Multi-mode vortex and wake-induced vibrations of a flexible cylinder in tandem arrangement. *Journal of Fluids and Structures*, **66**, 571-588.
DOI: 10.1016/j.jfluidstructs.2016.07.019
- Huera-Huarte FJ, Bearman PW, 2009a. Wake structures and vortex-induced vibrations of a long flexible cylinder—part 1: dynamic response. *Journal of Fluids and Structures*, **25**(6), 969-990.
DOI: 10.1016/j.jfluidstructs.2009.03.007
- Huera-Huarte FJ, Bearman PW, 2009b. Wake structures and vortex-induced vibrations of a long flexible cylinder—part 2: drag coefficients and vortex modes. *Journal of Fluids and Structures*, **25**(6), 991-1006.
DOI: 10.1016/j.jfluidstructs.2009.03.006
- Huera-Huarte FJ, Bearman PW, Chaplin JR, 2006. On the force distribution along the axis of a flexible circular cylinder undergoing multi-mode vortex-induced vibrations. *Journal of Fluids and Structures*, **22**(6), 897-903.
DOI: 10.1016/j.jfluidstructs.2006.04.014
- Jasak H, 2009. Dynamic mesh handling in OpenFOAM, *47th AIAA Aerospace Sciences Meeting Including the New Horizons Forum and Aerospace Exposition*, Orlando, 1-10.
DOI: 10.2514/6.2009-341
- Klaycham K, Athisakul C, Chucheepsakul S, 2016. Nonlinear vibration of marine riser with large displacement. *Journal of Marine Science and Technology*, **22**(2), 361-375.
DOI: 10.1007/s00773-016-0416-8
- Lie H, Kaasen KE, 2006. Modal analysis of measurements from a large-scale VIV model test of a riser in linearly sheared flow. *Journal of Fluids and Structures*, **22**(4), 557-575.
DOI: 10.1016/j.jfluidstructs.2006.01.002
- Lucor D, Imas L, Karniadakis GE, 2001. Vortex dislocations and force distribution of long flexible cylinders subjected to sheared flows. *Journal of Fluids and Structures*, **15**(3), 641-650.
DOI: 10.1006/jfls.2000.0366
- Menter FR, 1994. Two-equation eddy-viscosity turbulence models for engineering applications. *AIAA Journal*, **32**(8), 1598-1605.
DOI: 10.2514/3.12149
- Menter FR, Kuntz M, Langtry R, 2003. Ten years of industrial experience with the SST turbulence model. Hanjalic K, Nagano Y, Tummers M (Eds.), *Turbulence, Heat and Mass Transfer 4*. Begell House Inc.
- Monreal-Jiménez C, Oviedo-Tolentino F, Gutiérrez-Urueta GL, Romero-Méndez R, Mejía-Rodríguez G, 2016. Fluid forces on a flexible circular cylinder in vortex-induced vibrations. *Recent Advances in Fluid Dynamics with Environmental Applications*, Springer International Publishing, 37-50.
DOI: 10.1007/978-3-319-27965-7_4
- Pavlovskaja E, Keber M, Postnikov A, Reddington K, Wiercigroch M, 2016. Multi-modes approach to modelling of vortex-induced vibration. *International Journal of Non-Linear Mechanics*, **80**, 40-51.
DOI: 10.1016/j.ijnonlinmec.2015.11.008
- Rahman MAA, Leggoe J, Thiagarajan K, Mohd MH, Paik JK, 2016. Numerical simulations of vortex-induced vibrations on vertical cylindrical structure with different aspect ratios. *Ships and Offshore Structures*, **11**(4), 405-423.
DOI: 10.1080/17445302.2015.1013783
- Song L, Fu S, Dai S, Zhang M, Chen Y, 2016. Distribution of drag force coefficient along a flexible riser undergoing VIV in sheared flow. *Ocean Engineering*, **126**, 1-11.
DOI: 10.1016/j.oceaneng.2016.08.022
- Srinil N, 2010. Multi-mode interactions in vortex-induced vibrations of flexible curved/straight structures with geometric nonlinearities. *Journal of Fluids and Structures*, **26**(7), 1098-1122.
DOI: 10.1016/j.jfluidstructs.2010.08.005
- Trim AD, Braaten H, Lie H, Tognarelli MA, 2005. Experimental investigation of vortex-induced vibration of long marine risers. *Journal of Fluids and Structures*, **21**(3), 335-361.
DOI: 10.1016/j.jfluidstructs.2005.07.014
- Wang E, Xiao Q, 2016. Numerical simulation of vortex-induced vibration of a vertical riser in uniform and linearly sheared currents. *Ocean Engineering*, **121**, 492-515.
DOI: 10.1016/j.oceaneng.2016.06.002
- Wilcox DC, 1993. *Turbulence modeling for CFD*. DCW Industries, Inc., La Canada, USA, 20-80.
- Willden RHJ, Graham JMR, 2001. Numerical prediction of VIV on long flexible circular cylinders. *Journal of Fluids and Structures*, **15**(3), 659-669.
DOI: 10.1006/jfls.2000.0359
- Willden RHJ, Graham JMR, 2004. Multi-modal vortex-induced vibrations of a vertical riser pipe subject to a uniform current profile. *European Journal of Mechanics-B/Fluids*, **23**(1), 209-218.
DOI: 10.1016/j.euromechflu.2003.09.011
- Willden RHJ, Graham JMR, 2006. Three distinct response regimes for the transverse vortex-induced vibrations of circular cylinders at low Reynolds numbers. *Journal of Fluids and Structures*, **22**(6), 885-895.
DOI: 10.1016/j.jfluidstructs.2006.04.005
- Willden RHJ, Graham JMR, Giannakidis G, 2001. Vortex-induced vibration of single and multiple risers in a sheared current. *Proceedings of the Eleventh International Offshore and Polar Engineering Conference*, Stavanger, 406-410.